

On the momentum-dependent K^- -nuclear potentials

L. Dang¹, L. Li^{1y}, X. H. Zhong^{2z}, and P. Z. Ning^{1x}

¹Department of Physics, Nankai University, Tianjin 300071, China

²Institute of High Energy Physics, Chinese Academy of Sciences, Beijing 100039, China

The momentum-dependent K^- -nucleus optical potentials are obtained based on the RMF theory. The K^- mean free paths in normal nuclear matter and finite nuclei are predicted. By comparing the K^- mean free paths with those calculated from K^-n/K^-p scattering, we suggest that the real potential depth is $V_0 = 80$ MeV, and the imaginary potential parameter is $W_0 = 65$ MeV. The mean free paths in nuclei ^{12}C and ^{40}Ca are about 1–1.5 fm, which increases with increasing momentum in the region of $P_k < 0.625$ GeV. The elastic differential cross sections for K^- - ^{12}C and K^- - ^{40}Ca at the momentum $P_k = 300, 450, 600$ MeV are predicted as well, respectively. They are useful to the experiments.

PACS numbers: 21.65.+f, 21.30.Fe

I. INTRODUCTION

Recently kaon nuclear physics is a hot topic of nuclear physics. Especially the topic on the deeply bound K^- -nucleus states (i.e. kaonic nuclei) is the focus of attention in the recent years [1, 2, 3, 4, 5, 6, 7, 8, 9, 10, 11, 12, 13, 14, 15, 16, 17, 18, 19, 20, 21]. Whether they can be found in experiment or not is still a question should be answered by theorists and experimenters. All the questions around "kaonic nuclei" arise from the very different predictions on the kaon nucleus optical potentials in theory and the insufficient information on kaon-nucleus interactions from experiments.

The previous information of kaon-nucleus interactions in experiments come from the data of kaonic atoms. Using these data, Friedman, Gal et al. predicted a very strong attractive real potential, which reaches to 150–200 MeV at normal nuclear density. And the imaginary part predicted by them is about 50–70 MeV [22, 23]. However, the chiral model with a much shallower real potential (50 MeV) also fitted the data very well [24]. The reason is that the K^- -meson is only sensitive to the surface structure of nuclei, whether the potential inner the nuclei is deep or shallow has less effect on the theoretical prediction. Thus the K^- -atom data can not give us enough information on the kaon-nucleus interaction.

The information on kaon-nucleus interactions can also be obtained from K^-N scattering data. Analyzing K^-N scattering amplitude, Sibirtsev et al. predicted that the kaon-nucleus interaction has "momentum dependence" [25]. They have obtained a momentum-dependent potential in a dispersion approach at normal nuclear density. They predicted that the potential depth at zero momentum is about 140–200 MeV, decreases rapidly for

higher momenta. In our previous work [26] we have also found that the kaon nucleus optical potential has strong momentum dependence by fitting the only experimental data on the K^-C , K^-Ca scattering at the K^- incidence momentum $P_k = 800$ MeV/c [27]. We predicted the depth of real potential at the inner of finite nuclei is (45–55) MeV at $P_k = 800$ MeV/c, it is much shallower than that at zero momentum in the RMF. To study the momentum-dependent kaon nucleus potentials further, more experiments on K^- -nucleus scattering at different K^- incidence momenta $P_k < 800$ MeV/c are needed.

On the dynamics of the K^- -nucleus interaction, although there are some theoretical models, such as the chiral perturbation theory (ChPT) [28, 29], the density-dependent optical potential (DD) model [22, 23], the relativistic mean-field theory (RMF) model [30, 31, 32, 33], and the chiral unitary model [24, 34], their predictions are very different. Some of the models have considered the momentum dependence of the K^- -nucleus interaction, while most of them only give the kaon nucleus optical potential at zero momentum. If we use the scattering data, momentum-dependent potential is very essential to give compatible result with experiment. Thus, more theoretical studies are needed on the K^- -nucleus interaction, especially on the momentum dependence of K^- -nucleus potential, that is the purpose of the present work.

Based on the usual RMF model, one cannot get the corrected momentum dependence of K^- -nucleus interaction, and have to consider the internal structure of kaon-meson to introduce a momentum-dependent "form factor". When one extend the RMF to studying the K^-N interaction, they usually make an approximation, and u - d mesons are exchanged between the u - d quarks or their anti-quarks in kaon meson, and ignore the interaction with s quark. In this work, we consider a kaon meson as a two quarks system to introduce an exponential "form factor", $\exp(-P_k^2/4\Lambda^2)$, which modify the couplings. In fact, the "form factor" of an exponential form are widely adopted [35, 36, 37], which improved the calculations.

With the exponential "form factor", we can obtain the real part of the "momentum-dependent" kaon nucleus potential. Similarly, we believe that an exponential "form

E-mail: d1030115@mail.nankai.edu.cn

^yE-mail: lilei@mail.nankai.edu.cn

^zE-mail: zhongxh@ihep.ac.cn

^xE-mail: ningpz@mail.nankai.edu.cn

factor" $\exp(-P_k^2/4^2)$ is also needed in the imaginary part. Here two additional parameters and are introduced, which are determined by fitting the K^- -nucleus scattering data [27]. Next, with the momentum dependent potential we calculate the K^- mean free path in nuclear matter at normal nuclear density. By comparing our theoretical predictions of the K^- mean free paths with that calculated from $K^- p/K^- n$ total cross sections [38], the possible potential depths are constrained further. We find that the most possible real potential depth is $V_0 = 80$ MeV, and the most possible imaginary potential parameter is $W_0 = 65$ MeV. Finally, using the determined parameters, we predict the K^- mean free paths in nuclei, and the elastic scattering sections for K^- ^{12}C , K^- ^{40}Ca at $P_k = 300, 450, 600$ MeV, which may be useful for the future experiments.

The paper is organized as follows. In the subsequent section we introduce a momentum dependent kaon-nucleus optical potentials and determine the parameters. Then the K^- mean free paths in nuclear matter and finite nuclei are calculated, and the appropriate potential depths are also suggested in Sec. III. K^- -nucleus elastic differential cross sections for ^{12}C and ^{40}Ca are calculated in Sec. IV. Finally a brief conclusion is given in Sec. V.

II. MOMENTUM DEPENDENT OPTICAL POTENTIALS

The momentum dependent K^- -nucleus optical potential is crucial to studying K^- -nucleus scattering and the mean free paths of K^- in nuclear medium. Based on the RMF, the primary K^- -nucleus effective potential cannot give the corrected momentum dependence. Generally, the internal structure of kaon-meson becomes more and more important when its momentum becomes larger. In this work, we attempt to consider the internal structure of kaon-meson in the RMF, then a "form factor" will be added phenomenally to modify the coupling vertexes. From our calculations, we find that this correction can give the reasonable momentum dependence of K^- -nucleus optical potential.

A. the real part

In the following, we consider a kaon meson as a two quarks system and try to deduce a momentum dependent "form factor" to modify coupling vertexes within the framework of the RMF.

In the RMF, the $K^- N$ interactions are realized by exchanging scalar meson and vector meson π [19]. In the quark level, π - and π -mesons are exchanged between the u/d quarks or their anti-quarks. See Fig. 1, the scalar and vector couplings are given by

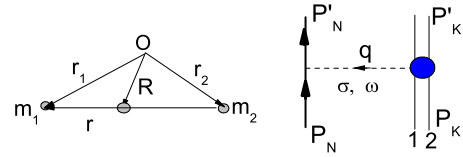


FIG. 1: Feynman diagram for the $K^- N$ interactions and internal coordinate of two quark system

$$L = g_K m_K K \bar{K}; \quad (1)$$

$$L_1 = ig_{\pi K} \pi \bar{K} + H.C.; \quad (2)$$

Replacing the scalar meson π and vector meson π with their plane wave form, we have

$$L = g_K m_K K \bar{K} e^{iq \cdot r_2} \bar{K}; \quad (3)$$

$$L_1 = ig_{\pi K} \pi \bar{K} e^{iq \cdot r_2} \bar{\pi} \bar{K} + H.C.; \quad (4)$$

we take $q = \alpha P_k$ approximately as the transferred momentum is proportional to K^- incidence momentum. Here r_2 represents the coordinate of u/d quarks, which can be related to the central mass coordinate R and the relative coordinate r in the quark model:

$$r_2 = R - \frac{m_2}{m_2} r; \quad (5)$$

where $m_2 = m_u$ and $\bar{\pi} = m_u m_s = (m_u + m_s)$. Thus, we have

$$e^{iq \cdot r_2} = e^{icP_K \cdot R} e^{\frac{c^2 P_K^2}{2(m_u - \bar{\pi})^2} \frac{icP_K}{m_2} r}; \quad (6)$$

On the harmonic-oscillator basis, the relative coordinate r in the second-quantized form are written,

$$r = \frac{1}{p} (a^\dagger + a) \quad (7)$$

where $\omega^2 = \omega_h^2$, ω_h is the harmonic-oscillator frequency. Then, we obtain

$$e^{iq \cdot r_2} = e^{icP_K \cdot R} e^{\frac{c^2 P_K^2}{2(m_u - \bar{\pi})^2} \frac{icP_K}{m_2} r} e^{\frac{a^\dagger}{2} \frac{icP_K}{m_2} a} e^{\frac{a^\dagger}{2} \frac{icP_K}{m_2} a}; \quad (8)$$

Finally, approximately we have

$$L = g_K m_K F(P_k^2) K \bar{K} a e^{icP_K \cdot R}; \quad (9)$$

$$L_1 = ig_{\pi K} F(P_k^2) K \bar{\pi} \bar{K} a^\dagger e^{icP_K \cdot R} + H.C.; \quad (10)$$

with

$$F(P_k^2) = \exp[-P_k^2/(4^2)]; \quad (11)$$

where

$$2^2 (m_u = c)^2; \quad (12)$$

$$and P_k = \sqrt{P_k^2}$$

In the central mass coordinate of K^- meson, we replace $a e^{i \vec{P}_k \cdot \vec{R}}$ and $a_1 e^{i \vec{P}_k \cdot \vec{R}}$ with 1 and 0 , respectively. One obtains

$$L' = g_K F(P_k^2) m_K K K; \quad (13)$$

$$L_1 = i g_{K\bar{K}} F(P_k^2) K \bar{K} K \bar{K} 0; \quad (14)$$

Naturally, we do not expect the naive quark model gives an appropriate value for the parameter g_K . In the calculation, the parameter are determined by fitting the experimental K^- -nucleus scattering data. From Eqs. (13, 14), we found that an additional factor $F(P_k^2)$ appears in the vertex compared with that without considering the internal structure of K^- meson. With the increasing momentum P_k , the factor becomes more and more important. Thus, considering the internal structure of K^- meson, the usual RMF Lagrangian for K^-N interaction should be modified as

$$L_K = \bar{K} \bar{K} m_K^2 K K - g_K m_K F(P_k^2) K K - i g_{K\bar{K}} F(P_k^2) K \bar{K} K \bar{K} 0 + g_{K\bar{K}} F(P_k^2) K \bar{K} K \bar{K} 0; \quad (15)$$

From the above Lagrangian, we can obtain the real part of the K^- -nucleus optical potential, which is

$$ReU = \frac{K}{2m_K}; \quad (16)$$

with the anti-kaon self-energy

$$\begin{aligned} K = & F(P_k^2) g_K m_K 0 - 2g_{K\bar{K}} E_K 0 \\ & F(P_k^2) (g_{K\bar{K}} 0)^2; \end{aligned} \quad (17)$$

which is related to the kaon-meson three momenta by the form factor $F(P_k^2)$. The K^- -meson energy E_K can be deduced from the RMF [19], which is given by

$$E_K = \frac{q}{m_K^2 + g_K F(P_k^2) m_K 0 + P_k^2} - g_{K\bar{K}} F(P_k^2) 0; \quad (18)$$

B. the imaginary part

So far, we ignored the anti-kaon meson absorption in the nuclear medium, which requires a complex potential. Within the framework of the RMF model, the imaginary potentials cannot be obtained directly. In order to include the effects of the anti-kaon meson absorption in

the nuclear medium, and make a more realistic estimation for the calculated results, we assume a specific form in imaginary potential, which is given by

$$\text{Im } U = f \cdot E(P_k^2)^2 \cdot \frac{E_K}{m_K} W_0 = 0; \quad (19)$$

with

$$F_2(P_k^2) = e^{P_k^2/(4^2)}; \quad (20)$$

which is also introduced to modify the imaginary potential (i.e. decay widths) as did in the real one. For the decay width $/M^2/g^2$, where M is the decay amplitude, and g is the coupling, the square of the "form factor" $F_2(P_k^2)^2$ is needed. And the parameter can be determined by fitting the experimental K^- -nucleus scattering data. In Eq. 19, W_0 is the depth of the imaginary potential at zero momentum in the usual models, such as DD and chiral models, which will be discussed later.

On the other hand, the phase space available for the decay products should be considered, which affects the imaginary potentials (widths). Thus, a factor, f , multiplying imaginary potentials $\text{Im } U$ is introduced in our calculations. Following the work in Ref. [8], two main decay channels are considered in the K^- decay mode. One is the mesonic decay channel, $K^- N \rightarrow \pi^- \bar{N}$. The corresponding factor is given by

$$f_1 = \frac{M_{01}^{3/2}}{M_1^{3/2}} \frac{q}{\frac{[M_{1/2}^2 (m_K + m_Y)^2] M_{1/2}^2 (m_Y - m_N)^2}{[M_{01}^2 (m_K + m_Y)^2] M_{01}^2 (m_Y - m_N)^2}} (M_1 - m_N - m_Y); \quad (21)$$

where $M_{01} = m_K + m_N$; $M_1 = m_N + E_K$, and $Y = \pi^- \bar{N}$. The other channel is the non-mesonic decay channel, $K^- N \rightarrow Y N$, and the corresponding factor is:

$$f_2 = \frac{M_{02}^{3/2}}{M_2^{3/2}} \frac{q}{\frac{[M_{2/2}^2 (m_N + m_Y)^2] M_{2/2}^2 (m_Y - m_N)^2}{[M_{02}^2 (m_N + m_Y)^2] M_{02}^2 (m_Y - m_N)^2}} (M_2 - m_N - m_Y); \quad (22)$$

where $M_{02} = m_K + 2m_N$; $M_2 = m_N + 2E_K$. Since final states dominate both the mesonic and non-mesonic decay channels [39], in the calculations, the hyperon Y is set as $Y = \pi^- \bar{N}$. The factor f can be assumed a mixture of 80% mesonic decay and 20% non-mesonic decay [8, 9, 39], thus $f = 0.8f_1 + 0.2f_2$.

From Eq. (19), we can see that the imaginary potential is related to the real part by the factor f .

C. determining the parameters and

In the calculations, the values of coupling constants $g_K = 2.088$ and $g_{K\bar{K}} = 3.02$ are adopted, which are most used in the RMF [19]. The imaginary potential parameter, W_0 , is not determined well. By fitting the K^- -atom data, $W_0 = 50$ MeV, however, the predictions in Refs. [20, 21] give a much deep value $W_0 = 100$ MeV. Thus, when we determine the parameters and , three

TABLE I: The parameters in the real and imaginary potential. The potentials are given in MeV and the parameter ρ in GeV.

g_K	$g_{\pi K}$		W_0	V_0
2.088	3.02	0.275	0.49	50
—	—	—	0.46	60
—	—	—	0.43	70
—	—	—	0.42	80
1.044	3.02	0.285	0.44	65
2.088	—	0.275	—	99
5.44	—	0.255	—	146

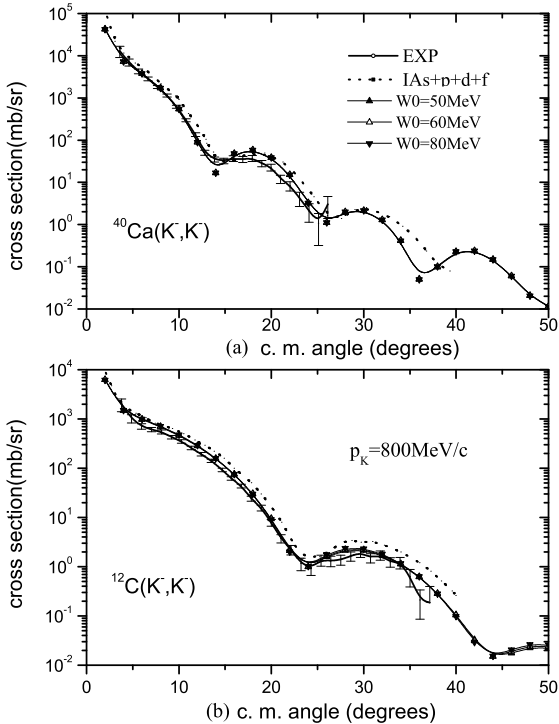


FIG. 2: The elastic differential cross section for K scattering from ^{40}Ca and ^{12}C at $p_K = 800$ MeV/c are shown in Fig. (a) and (b), respectively. The experimental data are from Ref. [27]. The triangles solid lines represent our calculations with the different imaginary depths, the dotted lines are the best results from Ref. [40].

cases $W_0 = 50, 60, 80$ MeV are taken into account, respectively.

The experimental data of the differential elastic cross sections for $K -^{12}\text{C}$ and $K -^{40}\text{Ca}$ at $p_K = 800$ MeV/c [27] are used to determine the parameters g_K and $g_{\pi K}$. In Fig. 2, with the optical potentials deduced in equations (16) and (19), the experimental data are fitted very well. For considering three cases $W_0 = 50, 60, 80$ MeV, three values for ρ are obtained, they are listed in Table I. Although the imaginary depths of the optical potentials are different, the experimental data can be fitted very well

by adjusting ρ . The reason is that the $K -\text{nucleus}$ interactions only occur on the surface of the nuclei, the $K -\text{mesons}$ nearly do not feel any effects from the inner of the nuclei. For comparison, we also presented the best theoretical predictions of Ref. [40] for the differential elastic cross sections of $K -^{12}\text{C}$ and $K -^{40}\text{Ca}$ at $p_K = 800$ MeV/c in Fig. 2. Where the impulse approximation potential (including up to f waves) are adopted. It is obvious that our results are better.

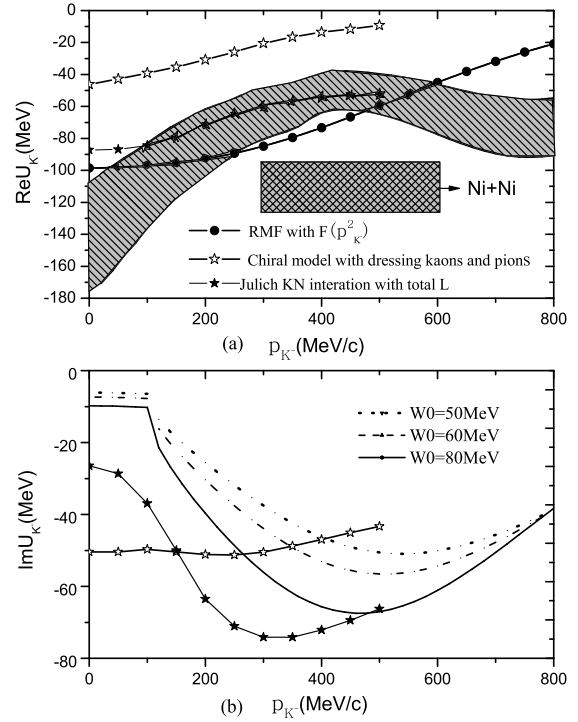


FIG. 3: The real and imaginary anti-kaon optical potentials of different models in normal nuclear matter are shown in Fig. (a) and (b), respectively. The solid and hollow pentagons lines represent the potential based on the Julich KN interaction [41] and the chiral model [42] (the anti-kaons and pions are dressed self-consistently), respectively. The shadow region between two solid curves is the result predicted by Sibirtsev and Cassing (SC model) [25], and the crossed rectangle indicates the results from the analysis of K production in $\text{Ni} + \text{Ni}$ collisions [30, 43].

With the determined parameters, we plotted the potentials at normal nuclear density as functions of kaon three momentum p_K in Fig. 3. The real and imaginary parts are shown in Fig. 3(a) and (b), respectively. For comparison, the potentials predicted by the others are also presented in Fig. 3. The solid pentagons curves are the predictions of a meson-exchange model with the Julich KN interaction (Julich model) [41]. The hollow pentagons curves are the results based on the lowest-order meson-baryon chiral lagrangian (the anti-kaons and pions are dressed self-consistently) (chiral model) [42].

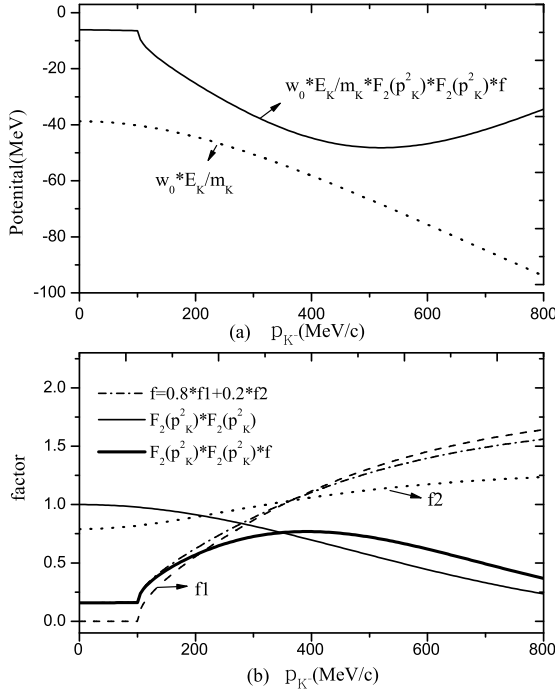


FIG. 4: The imaginary potential with and without factors as functions of the momentum are shown in Fig. (a), where $W_0 = 50$ MeV, and the corresponding factors in the imaginary potential varied with the momentum are shown in Fig. (b).

The shadow region between two solid curves are the result predicted by Sibirtsev and Cassing (SC model) [25], which excludes the repulsive low-energy resonance contribution in the scattering amplitude and averages over the fermion momentum. And the crossed rectangle indicate the results from the analysis of K^- production in $N + N$ i collisions [30, 43].

From the figure, we can see that our predictions on real potentials decrease with increasing momentum, the tendency is agreement with the other models [25, 41, 42]. The depths predicted by us are deeper than those of chiral and Julich model. In these models, chiral model gives much shallower real potential depths than the other three models. The predictions of Julich model, SC model and RMF model (our model) are compatible at $p_K < 600$ MeV, which are nearly in the possible region predicted with SC model.

Our results of the imaginary potentials firstly increase with increasing momentum till to $p_K = 450 - 550$ MeV and then decrease with momentum. The variational tendency is very similar with the predictions in Ref. [41]. There is a plateau for imaginary potential in the low energy $p_K < 100$ MeV region. Which indicates that the total-energy ($M_N + E_K$) is less than the threshold of π^- , and the decay channel $N \rightarrow K^- + \pi^+$ is closed. With the factor f , the imaginary potential depth are drastically suppressed from 50 - 80 MeV to 10 MeV at zero momentum and

normal nuclear density. To see the effects of f and form factor $F_2(p_K^2)$, these factors are shown as functions of p_K in Fig. 4. From the figure, we can see that the values of $F_2(p_K^2)$ decrease, while the values of f increase with increasing momentum. As a whole, the predictions with and without the factors are very different (see Fig. 4 (a)).

III. K MEAN FREE PATHS

For little experimental information directly from the inner nuclei, there are much uncertainties in both the real potentials and the imaginary parts. In this section, with our determined momentum-dependent K^- nucleus potentials, the K^- mean free paths in nuclear matter and finite nuclei are calculated. On the other hand we estimated the K^- mean free paths in nuclear matter according to the experimental data of the total cross sections for $K^- p$ and $K^- n$ [38]. By comparing the results from the two different approach, we expect to find more constraints for the $K^- N$ interactions.

A. The formula

The details of how to calculate a particle's mean free path in nuclei are given in our previous work [45], only the main formula are yielded here. To calculate the K^- mean free path, we must start from the K^- motion equation, which is [19],

$$r^2 \frac{d^2}{dr^2} E_K^2 + m_K^2 + \frac{1}{r} \frac{d}{dr} E_K = 0; \quad (23)$$

From it, a non-relativistic form can be obtained,

$$\frac{k^2}{2m_K} + U_K = E_K \quad m_K + \frac{(E_K - m_K)^2}{2m_K} \quad (24)$$

where U_K is the complex potential, which yields

$$U_K = \text{Re}U + i\text{Im}U; \quad (25)$$

where $\text{Re}U$ and $\text{Im}U$ are given in Eq. (16) and Eq. (19) respectively.

Since the potential U_K is complex, the anti-kaon momentum k is also complex and can be expressed as $k = k_R + ik_I$. Then, the anti-kaon mean free path, κ_K , is related to the imaginary part of the anti-kaon momentum by $\kappa_K = 1 = j2k_I j$. It is easy to derive an analytical expression for κ_K ,

$$\kappa_K = \frac{1}{\frac{1}{2} \frac{m_K}{m_K + B} + \frac{(\text{Im}U)^2}{(m_K + B)^2}}; \quad (26)$$

where, $B = E_K - m_K - \text{Re}U + (E_K - m_K)^2/2m_K$.

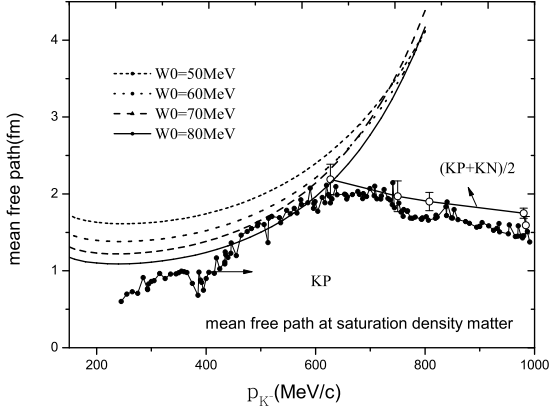


FIG. 5: The anti-kaon mean free paths corresponding to the different imaginary potentials are as functions of the incident momentum, p_K , from 150 MeV/c to 800 MeV/c in normal nuclear matter. And the mean free path corresponding to experimental Kp and $(Kp + Kn)/2$ total cross sections are also shown.

B. results and analysis

With the complex potential predicted in section II, we calculated the K mean free path in symmetric nuclear matter at normal nuclear density ρ_0 . The results are shown in Fig. 5. The short dashed, dotted, dashed and solid lines are corresponding to the imaginary depths $W_0 = (50; 60; 70; 80)$ MeV, respectively.

On the other hand the mean free path of K is related to the Kp/Kn scattering data by a simple relation $\lambda = \frac{1}{2} \cdot W$ where $\lambda = (\kappa_n + \kappa_p)/2$ is the average of the total Kn and Kp cross sections. There are some Kp scattering data in the range of $0.24 < p_K < 1$ GeV, and no data for Kn scattering in $p_K < 0.6$ GeV. Thus only the mean free paths obtained from $\lambda = (\kappa_n + \kappa_p)/2$ in the region of $0.6 < p_K < 1$ GeV are shown in Fig. 5. According to the Kp cross section data, the values of $\lambda = (\kappa_p)$ can be estimated as well. From the figure, we find that $\lambda_p > \lambda_n$, and λ_p is a little larger than λ_n . Thus we believe $\lambda_p > \lambda_n$ in the region of $p_K < 0.6$ GeV.

The range of p_K (1.0–0.3) GeV corresponds to a resonance region, our model can not give reasonable mean free paths in this region. From Fig. 5, we can see that the predicted mean free paths increase with increasing K momentum, the variational tendency is agreement with that calculated from Kp cross sections in the region of $p_K < 0.65$ GeV.

In the region of $0.46 < p_K < 0.6$ GeV, we find that the predicted mean free paths with $W_0 = 80$ MeV are smaller than those calculated from Kp cross sections. Considering the fact $\lambda_p > \lambda_n$, we believe the imaginary parameter $W_0 = 80$ MeV may be too large. While, with $W_0 = 50$ MeV it seems to give too large mean free paths

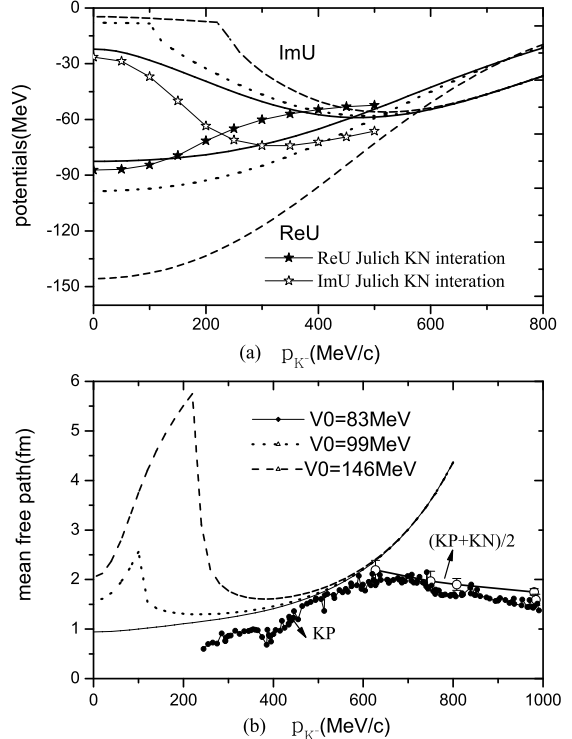


FIG. 6: The λ of the different real depths varied with the incident momentum, p_K , from 0 MeV/c to 800 MeV/c in normal nuclear matter. And the corresponding K optical potentials are shown in Fig. a.

in the whole region, which indicates that $W_0 = 50$ is too small. With the conditions $\lambda_p > \lambda_n$ and $\lambda_p > \lambda_n$, the imaginary depth parameter W_0 should be $(60-5)$ MeV.

However, when $0.24 < p_K < 0.4$ GeV the imaginary part $W_0 = (60-5)$ may be too small, for the predicted mean free paths are a little larger than what one expects. The inconsistency may be overcome by adjusting the real potential depths in their possible region. As we know the real potentials have a large possible range from 50 MeV to 200 MeV predicted by different models. To see the effects of the real potential depths on the mean free path, here, we considered the coupling constant g_K as a free parameter. The different real potential depths can be obtained by adjusting g_K . For the imaginary potentials are related to real parts by the "form factor", corresponding to the different real parts they are different with the same parameter W_0 . With $W_0 = 65$ MeV, the mean free paths for the different real potential depths $V_0 = 83, 99, 146$ MeV are shown in Fig. 6(b). The corresponding potentials are shown in Fig. 6(a), and the parameters and are presented in the Tab. I, which are also determined by fitting the K nucleus scattering data at $p_K = 800$ MeV/c.

From the figure, we can see that the effects of the real

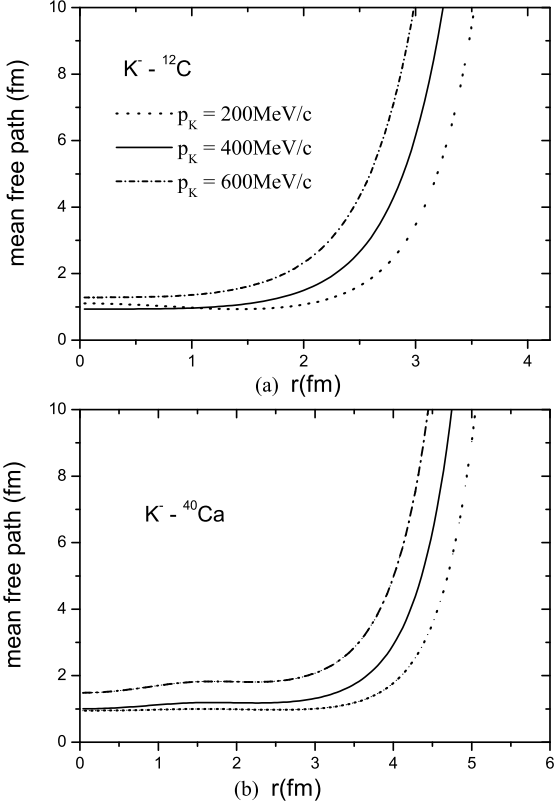


FIG. 7: The anti-kaon mean free path varied with the radius in ^{12}C and ^{40}Ca when the incident energies, $P_K = (200, 300, 600)$ MeV/c are shown in Fig. a and b, respectively.

potential depth on the mean free path are obvious. If we set $V_0 > 99$ MeV, our predictions of the K^- mean free paths are far from p (see the curve for $V_0 = 146$ MeV), while $V_0 < 99$ MeV the predictions become better. Thus, it indicates that the real potential depth should be shallower than 99 MeV. If we set $V_0 = 83$ MeV, which is just around the lower limit of the RMF, the predicted mean free paths are reasonable and the imaginary part $W_0 = 65$ MeV is no longer "too small" in the range of $0.24 < P_K < 0.4$ GeV. When $V_0 = 83$ MeV and $W_0 = 65$ MeV, both the real and imaginary potentials (the solid curves in Fig. 6(a)) predicted by us are very close to those of Jülich K^-N interactions [41] (the star curves in Fig. 6(a)) in the range of $P_K < 100$ MeV.

It is interesting that the recent experiment also indicated that the in-medium K^-N potential depth is on the order of 80 MeV at normal nuclear density. When assuming a K^-N potential depth of about 80 MeV, the calculations agree reasonably well with the ratio of invariant production cross sections of K^- mesons over K^+ mesons for $p + \text{Au}$ and, in average, also for $p + \text{C}$ [46].

On the other hand, in Fig. 6(b), we have noted that when the real potential depth is strong enough, a "peak" appears in the low momentum region of $P_K < 250$ MeV.

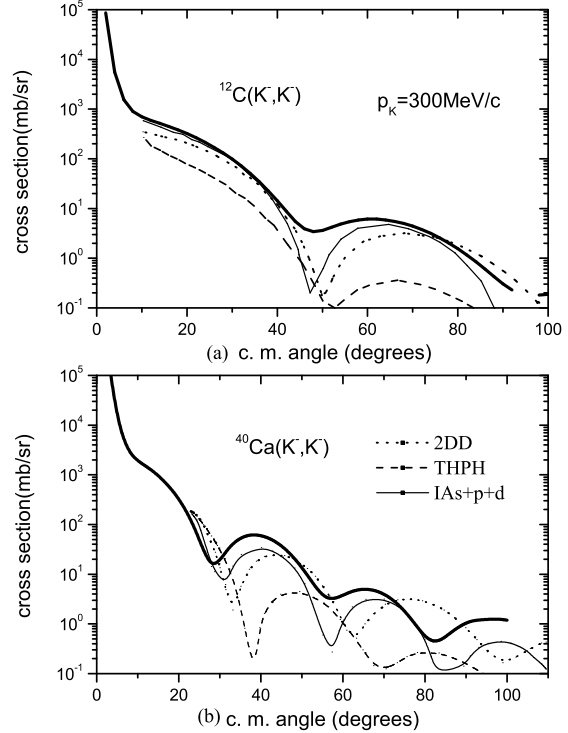


FIG. 8: The elastic differential cross section for K^- scattering from ^{40}Ca and ^{12}C at $P_K = 300$ MeV/c are shown in Fig. (a) and (b), respectively. The fat solid lines are the results of our momentum dependent potentials; the dotted lines, dash-dotted lines and dashed lines are the results from Ref. [40].

The position of the peak just corresponds to $M_N + E_K = M + M$. When $M_N + E_K < M + M$, the decay channel $K^-N \rightarrow \pi^- + \text{N}$ is forbidden. If it is the case, we believe that it should be seen in the experiments.

As a whole, with the constraints of the mean free path calculated from K^-N scattering data, we predicted that the real potential depth is $V_0 = 80$ MeV, and the imaginary parameter $W_0 = 65$ MeV. Using these potentials one can not only fitted the K^- -nucleus scattering data at $P_K = 800$ MeV/c but also gave the reasonable mean free paths.

Setting $V_0 = 83$ MeV, and the imaginary part $W_0 = 65$ MeV, the K^- mean free paths in ^{12}C and ^{40}Ca are calculated, they are shown in Fig. 7. From the figure, we can see that the K^- mean free paths in ^{12}C or ^{40}Ca are about 1 fm when $P_K = 200$ MeV, while when the momentum P_K increases to 600 MeV, the mean free paths increase to 1.5 fm. We expect there are some experiments on the K^- mean free paths in the future.

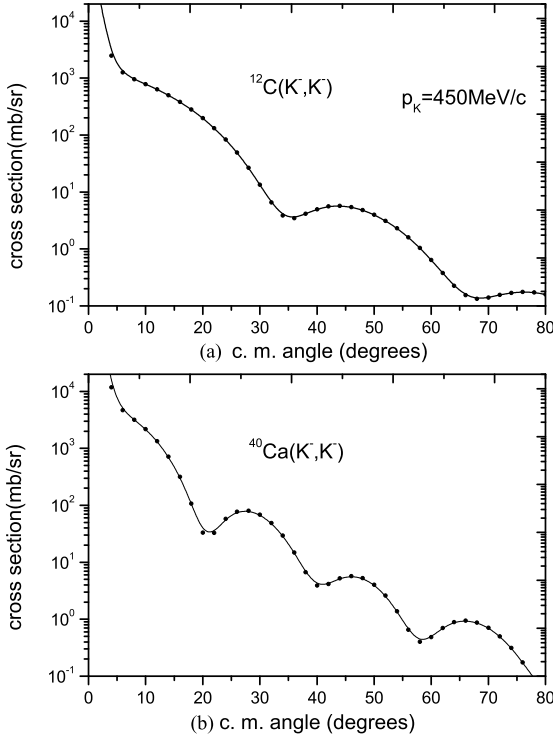


FIG. 9: Our calculations of the elastic differential cross section for K^- scattering from ^{40}Ca and ^{12}C at $p_K = 450 \text{ MeV}/c$ are shown in Fig. (a) and (b), respectively.

IV. K^- -NUCLEUS SCATTERING

Since the momentum-dependent potential is introduced, the parameters are also determined, and the potential depths for real and imaginary parts are suggested by us, which are expected to be tested in experiments. The K^- -nucleus scattering experiment may be a good method to test our predictions. Thus, in this section we gave the theoretical predictions of the elastic differential cross section for K^- - ^{12}C and K^- - ^{40}Ca at the momentum of $p_K = 300, 450, 600 \text{ MeV}$. The results are shown in Figs. 8-10, respectively. These calculations may be a guide to experiment on the K^- -nucleus scattering.

In the calculations, we set $V_0 = 83 \text{ MeV}$ and $W_0 = 65 \text{ MeV}$, and the parameters, determined by fitting the experiment data of K^- -nucleus scattering at $p_K = 800 \text{ MeV}/c$. The details on the K^- -nucleus scattering calculations can be found in our previous paper [26].

In Fig. 8, we show our theoretical predictions of the elastic differential cross section for K^- -nucleus scattering at $p_K = 300 \text{ MeV}/c$. For comparison, the results in Ref. [40] with different kaon-nucleus potentials are also presented. The solid lines are the results for the IA_{s+p+d} model, the dashed lines correspond to the results of the THPH model, and the dotted lines are for 2DD model. From the figure, our calculations are close to the results

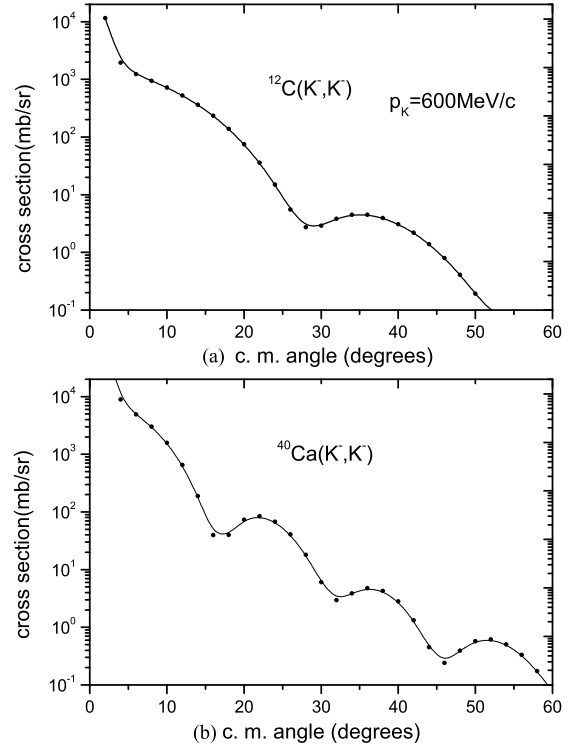


FIG. 10: The same as did in Fig. 9 at $p_K = 600 \text{ MeV}/c$.

of the IA_{s+p+d} model. We must emphasize the IA_{s+p+d} model is the best model to describe the experimental data in Ref. [40].

V. CONCLUSION

The momentum-dependent K^- -nucleus potentials are obtained based on the RMF. We think that the momentum dependence comes from the interior structure of a kaon-meson. By fitting the K^- -nucleus elastic differential cross sections for ^{12}C and ^{40}Ca at $p_K = 800 \text{ MeV}/c$, the parameters and are determined.

With the determined potentials, the K^- mean free paths in normal nuclear matter and nuclei are calculated. By comparing the theoretical predictions with the mean free paths calculated from K^- -nucleus scattering data, we found that the real potential depth should be $V_0 = 80 \text{ MeV}$, and the imaginary parameter should be $W_0 = 65 \text{ MeV}$. The mean free paths increase with increasing incident momentum in the range of $0 < p_K < 600 \text{ MeV}$, they are about 1.5 fm in nuclei and about 1.2 fm at the normal nuclear density.

One point must be emphasized, if our predictions about the potential depths ($V_0 = 80 \text{ MeV}$, $W_0 = 65 \text{ MeV}$) are true, according to our calculations in [19], the sum of the halfwidths of the $1s$ and $1p$ states are larger than their separations in K^- -nuclei. In other words, no

discrete K bound states in the A = 12 nuclei can be found in experiments.

The elastic differential cross sections for K^- - ^{12}C and K^- - ^{40}Ca at the momentum of $P_k = 300, 450, 600$ MeV are also predicted. We expect some experiments on the K^- -nucleus scattering for the low momentum region $P_k < 650$ MeV will be taken in the future.

by the Natural Science Foundation of China (Grant No. 10575054), China Postdoctoral Science Foundation, and the Institute of High Energy Physics, CAS.

Acknowledgements

X.H. Zhong would like to thank Prof. H. Oeschler for useful discussions. This work was supported, in part,

[1] A. Baca, C. Garcia-Recio, J. Nieves, Nucl. Phys. A 673, 335 (2000).
 [2] A. Cieply, E. Friedman, A. Gal, J. Mares, Nucl. Phys. A 696, 173 (2001).
 [3] M. Iwasaki, et al., Nucl. Instrum. Method Phys. Res. A 473, 286 (2001).
 [4] T. Yamazaki and Y. Akaishi, Phys. Lett. B 535, 70 (2002).
 [5] Y. Akaishi and T. Yamazaki, Phys. Rev. C 65, 044005 (2002).
 [6] A. Dote, H. Horiuchi, Y. Akaishi, and T. Yamazaki, Phys. Rev. C 70, 044313 (2004).
 [7] A. Dote, H. Horiuchi, Y. Akaishi, T. Yamazaki, Phys. Lett. B 590, 51 (2004).
 [8] J. Mares, E. Friedman, and A. Gal, Phys. Lett. B 606, 295 (2005).
 [9] J. Mares, E. Friedman, and A. Gal, Nucl. Phys. A 770, 84 (2006).
 [10] N. Agnello, G. Beer, L. Benussi, et al., Nucl. Phys. A 752, 139c (2005).
 [11] A. Dote, Y. Akaishi, T. Yamazaki, Nucl. Phys. A 754, 391c (2005).
 [12] J. Yamagata, H. Nagahiro, Y. Okumura et al., Prog. Theor. Phys. 114, 301 (2005).
 [13] E. Oset, H. Toki, Phys. Rev. C 74, 015207 (2006).
 [14] T. Suzuki, H. Bhang et al., Phys. Lett. B 597, 263 (2004).
 [15] T. Suzuki, H. Bhang et al., Nucl. Phys. A 754, 375c (2005).
 [16] T. Kishimoto, T. Hayakawa et al., Nucl. Phys. A 754, 383c (2005).
 [17] M. Agnello, G. Beer et al. [FINUDA Collaboration], Phys. Rev. Lett. 94, 212303 (2005).
 [18] V. K. M. Agas, E. Oset, A. Ramos and H. Toki, Phys. Rev. C 74, 025206 (2006).
 [19] X. H. Zhong, G. X. Peng, L. Li, P. Z. Ning, Phys. Rev. C 74, 034321, (2006).
 [20] N. V. Shevchenko, A. Gal, J. Mares, nucl-th/0610022
 [21] V. K. M. Agas, E. Oset, A. Ramos, H. Toki, nucl-th/0611098.
 [22] E. Friedman, A. Gal, C. J. Batty, Phys. Lett. B 308, 6 (1993); Nucl. Phys. A 579, 518 (1994).
 [23] E. Friedman, A. Gal, J. Mares, A. Cieply, Phys. Rev. C 60, 024314 (1999).
 [24] S. Hirenzaki, Y. Okumura, H. Toki, E. Oset, and A. Ramos, Phys. Rev. C 61, 055205 (2000).
 [25] A. Sibirtsev and W. Cassing, Nucl. Phys. A 641, 476, (1998); nucl-th/9909024
 [26] Xian-Hui Zhong, Lei Li, Chong-Hai Cai, Ping-Zhi Ning, Commun. Theor. Phys. 41, 573, (2004).
 [27] D. Marlow, et al., Phys. Rev. C 25, 2619 (1982).
 [28] D. B. Kaplan and A. E. Nelson, Phys. Lett. B 175, 57 (1986).
 [29] G. E. Brown and C. -H. Lee et al., Nucl. Phys. A 567, 937 (1994).
 [30] G. Q. Li, C. -H. Lee, and G. E. Brown, Nucl. Phys. A 625, 372 (1997).
 [31] J. Schacher, I. N. M. Mishustin, and J. B. Bondorf, Nucl. Phys. A 625, 325 (1997).
 [32] J. Schacher, A. Gal, I. N. M. Mishustin, H. Stöcker, and W. Greiner, Phys. Lett. B 334, 268 (1994).
 [33] J. Schacher and I. N. M. Mishustin, Phys. Rev. C 53 (1996) 1416.
 [34] E. Oset, D. Cabrera, V. K. M. Agas, L. Roca, S. Sarkar, M. J. Vicente Vacas and A. Ramos, Journal of physics, 53, 1 (1999).
 [35] Qiang Zhao, Phys. Lett. B 636 197 (2006); Q. Zhao, Phys. Rev. D 72, 074001 (2005); hep-ph/0508086; F. E. Close and Q. Zhao, Phys. Rev. D 71, 094022 (2005).
 [36] N. Isgur, D. Scora, B. Grinstein, and M. W. Wise, Phys. Rev. D 39, 789 (1989); F. E. Close and A. Wambach, Nucl. Phys. B 412, 169 (1994).
 [37] R. Kokoski and N. Isgur, Phys. Rev. D 35, 907 (1987).
 [38] W. -M. Yao et al., J. Phys. G 33, 1 (2006).
 [39] W. Wickens, D. N. Toovee, D. H. D avis, Nuovo Cimento A 39, 538 (1977).
 [40] C. G. Garcia-Recio, A. J. M. Elgaroy, and J. Nieves, Phys. Rev. C 67, 047601 (2003).
 [41] L. Tolos, A. Ramos, A. Polls, Thomas T. S. Kuo, Nucl. Phys. A 690, 547 (2001).
 [42] A. Ramos and E. Oset, Nucl. Phys. A 671 481 (2001).
 [43] W. Cassing and E. L. Bratkovskaya, Phys. Rep. 308, 65 (1999).
 [44] R. K. Norren, M. Prakash and P. J. Ellis, Phys. Rev. C 52, 3470 (1995).
 [45] Q. L. Wang, L. Dang, X. H. Zhong, C. Y. Song and P. Z. Ning, Europhys. Lett., 75, 36 (2006).
 [46] W. Scheinast et al., Phys. Rev. Lett. 96, 072301 (2006).